# Continuum Nanofluidics

Jesper S. Hansen,[*,†] Jeppe C. Dyre,[†] Peter Daivis,[‡] Billy D. Todd,[§] and Henrik Bruus[||]

[†]DNRF Centre "Glass and Time", IMFUFA, Department of Sciences, Roskilde University, Postbox 260, DK-4000 Roskilde, Denmark

[‡]Applied Physics, School of Applied Sciences, RMIT University, GPO Box 2476, Melbourne, Victoria 3001, Australia

[§]Department of Mathematics, Faculty of Science, Engineering and Technology, and Center for Molecular Simulation, Swinburne University of Technology, P.O. Box 218, Hawthorn, Victoria 3122, Australia

[||]Department of Physics, Technical University of Denmark, DTU Physics Building 309, DK-2800 Kongens Lyngby, Denmark

S *Supporting Information*

ABSTRACT: This paper introduces the fundamental continuum theory governing momentum transport in isotropic nanofluidic systems. The theory is an extension of the classical Navier−Stokes equation, and includes coupling between translational and rotational degrees of freedom as well as nonlocal response functions that incorporate spatial correlations. The continuum theory is compared with molecular dynamics simulation data for both relaxation processes and fluid flows, showing excellent agreement on the nanometer length scale. We also present practical tools to estimate when the extended theory should be used. It is shown that in the wall−fluid region the fluid molecules align with the wall, and in this region the isotropic model may fail and a full anisotropic description is necessary.
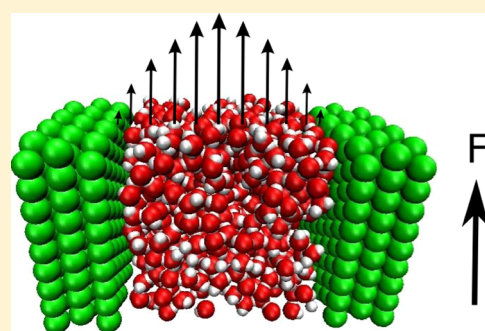
I. INTRODUCTION

Nanoscale devices can now be fabricated with channels where the smallest dimension is just a few nanometers,[1] and the development of nanofluidic theory[1−3] is more relevant than ever. Consider the following example. Perrson et al.[4] used a series of rectangular nanochannels with widths ranging from 14 to 300 nm to connect two microscale chambers. By means of capillary filling, fluid from one chamber fills up the channels and thus connects the two chambers. The filling rate was measured for different channel widths and for both Milli-Q water (filtered deionized water) and an electrolyte solution of sodium chloride. The rate did not follow the Washburn equation for channel widths smaller than 100 nm. The Washburn equation is based on the classical continuum picture[3] using Poiseuille's law of fluid motion, which includes the Newtonian (or macroscopic) shear viscosity. For widths larger than 100 nm the Washburn equation correctly predicts the filling rate. These findings are in accordance with the common understanding that the discrete nature of the fluid at small scales destroys the continuum picture.[5,6] In fact, many researchers categorize continuum physics as physics on the macroscopic scale; see for example ref 7. Several questions immediately arise: When exactly does the classical continuum picture fail? How is this breakdown manifested? Does the length scale of the breakdown depend on the specific problem? Can one improve the continuum description such that it applies on small scales?

Demanding sufficient smoothness of the macroscopic quantities with respect to time and position and using a simple statistical argument, Lautrup[7] estimates that the smallest volume accessible to the continuum description must contain at least 10^4 molecules. This corresponds to a length scale of 8−80 nm,

depending on the density. For steady flows the temporal fluctuations can be averaged out and the accessible volume is much smaller. This is illustrated in Figure 1, where we have performed
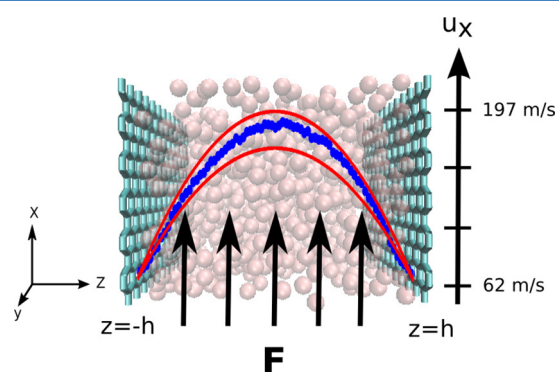
Figure 1. Comparison between atomistic simulations (blue filled circles) and the continuum prediction (red lines) for a methane fluid undergoing a Poiseuille flow. The flow is generated by an external force field with magnitude $F = 50$ TN, pointing along the x direction. The Navier−Stokes equation predicts a velocity profile of $u_x(z) = \rho F/(2\eta_0)(h^2 - z^2) + u_w$, where $\rho = 270$ kg m^{-3} is the mass density, $\eta_0 = 9.3 \pm 0.6$ μ Pa·s is the Newtonian shear viscosity, and $u_w = 62$ ms^{-1} is the fluid slip velocity at the wall surface. The two lines represent the interval associated with the standard error in the viscosity.[8] The width of the slit pore is approximately 10 molecular diameters or 3.3 nm.

an atomistic simulation (data given by blue filled circles) of a methane fluid confined between two graphene sheets undergoing Poiseuille flow. The slit pore has a width of approximately 3.3 nm, and the flow is driven by an external force field. The classical continuum prediction is plotted as two red lines illustrating the maximum and minimum profiles allowed within statistical uncertainty on the Newtonian shear viscosity.[8] Only the fluid slip velocity at the wall surface is used as a fitting parameter. For this system the continuum theory gives a satisfactory description of the fluid steady state velocity profile on a length scale of a few nanometers. Apparently, even on these small length scales the molecular structure and degrees of freedom can be coarsened into simple transport coefficients such as the viscosity. For water undergoing a steady flow it has been shown by atomistic simulations that the continuum description holds for channel widths of just 6−10 nm.[1,9] These results contrast earlier assumptions about the validity of the continuum picture and the statement that continuum physics is physics on the macroscopic scale.[5,7] Interestingly, it was later argued by Thamdrup et al.[10] that the disagreement between the experiment by Persson et al.[4] and the Washburn prediction is due to pinned microbubles resulting in an increase in hydraulic resistance.

At some point the classical continuum description will of course break down. To mention two examples, Travis et al.[11] showed that for atomic fluidic systems the velocity profile features modulations for confinements on the order of 5 atomic diameters. Decheverry and Bocquet[12] analyzed the effect of thermal fluctuations on the mass transport of fluid through a nanotube. When the classical continuum theory fails, the dynamics is frequently quantified by different transport coefficients compared to those of the bulk system, and effective transport coefficients are introduced into the continuum constitutive relations.[13,14]

The main point of this paper is that the observation of a breakdown need not be a failure of the continuum picture itself but rather a result of inadequate modeling wherein important dynamical processes are not accounted for by classical theories. A very well understood example is the effect of the Debye screening layer in electrolyte microflows.[3] Two other physical mechanisms that become important on the nanoscale are often ignored in the literature, however, and this paper will treat these in detail: (i) In classical hydrodynamics the fluid's local rotation is determined uniquely by the fluid streaming velocity. One can quantify the rotation from the local angular velocity field which is one-half the vorticity, that is, one-half the curl of the streaming velocity itself.[6] However, if the couple force, that is, the force component producing pure rotation, is large, then the rotation must be treated as an independent variable. The extended description is known as Cosserat (or micropolar) continuum mechanics,[15,16] first formulated by the Cosserat brothers[17,18] in the late 19th century. Cosserat continuum theory is used in various areas such as liquid crystal studies[19] and blood flows[20] and was studied intensively in the 1950s to 1970s; see refs 21−27. For some reason it is not, however, adopted by the nanofluidic community. We show that Cosserat theory must also be used for fluid flows in extremely small confinements where the molecular structure becomes important. (ii) Classical hydrodynamics is based on local constitutive relations relating fluxes to thermodynamic forces. For shear flow the stress at some point depends on the strain rate at that particular point. If the stress depends linearly on the strain rate, then this leads to the Newtonian law of viscosity.[6] A more general linear constitutive relation is to let the stress be a function of the entire strain rate history and spatial distribution, i.e., given by a spatial and tem-

poral convolution integral of a viscosity kernel and the strain rate.[28] This is the approach of generalized linear response theory.[29,30] The viscosity kernel accounts for the characteristic length scale of the spatial correlations;[31,32] we show later that this must be taken into account in order to arrive at the correct fluid response on molecular length scales.

Our presentation is based on comparisons of continuum predictions with atomistic molecular dynamics (MD) simulation data. These two descriptions are fundamentally different in two ways. First, in MD the system is characterized by discrete particles where the path of each individual particle constituting the fluid is traced out through classical mechanics;[33] i.e., the particle interactions must be known. The discretization of matter is, of course, in strong contrast to the fundamental assumptions of continuum mechanics. Second, the continuum description applies constitutive relations to form mathematical closed problems. No such models are enforced in the standard MD simulations. Any discrepancy between MD and the continuum description may therefore be a result of a breakdown of the constitutive relation rather than a breakdown of the continuum theory as such. Our basic conjecture is that MD acts as an idealized numerical experiment, and if a given continuum theory agrees with the MD data, then the theory correctly accounts for the phenomena we study.

Let us specify more accurately what is meant by continuum theory. Basically, one refers to deformable fluid volumes characterized by quantities which are continuous at any point $\mathbf{r}$ over the entire volume and at any time t.[6] This means that these quantities are described mathematically by field variables. The basic continuum hypothesis is that one can associate a given fluid subvolume (or "fluid particle") with the same characteristic quantities of the entire deformable fluid volume, no matter how small the subvolume.[5,6] Lautrup[7] suggests a lower limit on the order of 10^4 molecules as stated previously, but averaging allows an arbitrarily small fluid particle volume as seen in Figure 1. One field variable is the streaming velocity, which is the mass-weighted average velocity of the individual molecules in the fluid particle around a given point.[3] The fluid's dynamics is governed by balance (or conservation) equations. In general the balance equation for some quantity per unit mass, $\phi = \phi(\mathbf{r}, t)$, reads in the Eulerian differential form as[24]

$$\frac{\partial(\rho\phi)}{\partial t} + \nabla\cdot(\rho\mathbf{u}\phi) = \sigma_\phi - \nabla\cdot\mathbf{J}_\phi \tag{1}$$

where ρ is the mass density, σ_ϕ is a production term, $\mathbf{u}$ is the streaming velocity, and $\mathbf{J}_\phi$ is the flux of ϕ. Here ϕ can be a scalar or vector quantity. For $\phi = \mathbf{u}$, the right-hand side of eq 1 is the sum of the body force and the surface force densities, that is, forces per unit volume and eq 1 is the momentum balance equation. The body force density can be a gravitational-like force driving the flow as in Figure 1, and the surface force density is the pressure tensor $\mathbf{J}_u = \mathbf{P}$.[30] A special case is the mass balance equation for which $\phi = 1$. Since rotation is treated as an independent variable, a balance equation in the form of eq 1 must be formulated for rotation; this is done in the Supporting Information (SI). Importantly, in the extended Cosserat description the pressure tensor $\mathbf{P}$ need not be symmetric[21−24] as in the classical continuum theory.

A comparison between the continuum description and MD simulation data is carried out for molecular fluidic systems at equilibrium as well as for steady flows in a slit pore. Here we investigate four molecular fluids: a methane fluid, a generic diatomic (dumbbell) fluid, liquid butane, and liquid water. For

methane 75% of the mass is centered in the carbon nucleus, and methane is treated here to be a simple spherical point-mass molecule, as was done in Figure 1. Water will, on the other hand, be treated differently using the flexible SPC/Fw water model[34] that accounts for the molecular structure and hydrogen bonds and thus for the structure of liquid water. The butane model is a coarse-grained model where the methyl and methylene groups are each represented by a united atomic unit, i.e., a spherical point mass. Details about the butane model can be found in ref 35; however, here flexible bonds are implemented with parameters from the generalized Amber force field.[36] The simulations are done using the seplib library.[37]

Nanofluidic flows are often associated with fluid slippage at the wall boundary.[38] Just like the effect of the fluid−fluid interactions is lumped into a single parameter, e.g., viscosity, the effect from the fluid−solid interaction can be modeled into a friction coefficient determining the boundary slip. The slippage has a large effect on the flow rate in extreme confinement and is usually quantified by the slip length L_s. For a Hagen−Poiseuille flow in a tube with radius R, the relative flow enhancement ΔE^{rel} due to the slip is given as[39]

$$\Delta E^{\mathrm{rel}} = 1 + \frac{4L_s}{R} \qquad (2)$$

L_s is typically on the order of a few nanometers. Thus, for a given nonzero slip length the flow enhancement increases hyperbolically as the tube radius decreases. The slip is always present but has an insignificant effect on the flow rate for tube radii greater than micrometers. L_s is normally independent of system size; that is, it is not an intrinsic nanofluidic phenomenon and is therefore not addressed in this paper. Slippage is modeled here in an ad hoc fashion as was done in Figure 1.

In the SI we derive the Cosserat extended continuum theory from the microscopic point of view using a microscopic hydrodynamic operator. The derivation, which is based on the fundamental definition of the macroscopic field variables in terms of the corresponding molecular quantities, follows the ideas of Irving and Kirkwood[40] and Evans and Morriss;[30] see also ref 41. The derivation leads to a molecular interpretation of the fluxes entering eq 1. The final dynamical system of equations is sometimes referred to as the extended Navier−Stokes (ENS) equations; these are given by

$$\rho \frac{D\mathbf{u}}{Dt} = \boldsymbol{\sigma}_{\mathbf{u}} - \nabla p_{\mathrm{eq}} + \left(\eta_v + \frac{\eta_0}{3} - \eta_r\right)\nabla(\nabla\cdot\mathbf{u}) + (\eta_0 + \eta_r)\nabla^2\mathbf{u}$$
$$+ 2\eta_r\nabla\times\boldsymbol{\Omega} \qquad (3a)$$

$$\rho I \frac{D\boldsymbol{\Omega}}{Dt} = \boldsymbol{\sigma}_{\mathbf{S}} + 2\eta_r(\nabla\times\mathbf{u} - 2\boldsymbol{\Omega}) + \left(\zeta_v + \frac{\zeta_0}{3} - \zeta_r\right)\nabla(\nabla\cdot\boldsymbol{\Omega})$$
$$+ (\zeta_0 + \zeta_r)\nabla^2\boldsymbol{\Omega} \qquad (3b)$$

where D/Dt is the material operator, $\boldsymbol{\Omega}$ is the spin angular velocity field, ∇p is the pressure gradient, and I is the moment of inertia per unit mass. Transport coefficients η_v, η_0, and η_r are the bulk, shear, and rotational viscosities, respectively, and ζ_v, ζ_0, and ζ_r are the corresponding spin viscosities. Finally, inertia per unit mass. $\boldsymbol{\sigma}_{\mathbf{u}}$ and $\boldsymbol{\sigma}_{\mathbf{S}}$ represent production terms of linear and spin angular momentum, respectively. We refer the reader to the SI for a derivation and discussion of eq 3.

The theory is strictly correct only for isotropic systems, and we study such nanofluidics cases in sections II and III, comparing theoretical predictions with MD simulation data. Flows in extreme confinement, nanoflows, are characterized by strong density

inhomogeneities and anisotropy. We study such flows in section IV, again comparing theory with MD data. Finally, section V gives a brief summary.

II. COUPLING: MULTISCALE RELAXATION PHENOMENA IN MOLECULAR FLUIDS

The purpose of this section is to demonstrate the validity of the ENS equations, eqs 3, by comparing the predictions of different thermally induced relaxation phenomena with MD simulation data; \see also refs 42 and 43. We start with this problem instead of the situation with confining walls as the latter introduces density inhomogeneities and molecular alignment at the wall−fluid interface. We return to this more complex situation in section IV.

Rather than investigating the quantities directly, one typically studies the associated correlations.[44] Here we will use the approach based on Onsager's regression hypothesis,[45] which states that thermal perturbations on average decay according to the deterministic hydrodynamic equations of motion. Specifically, we will compare mechanical spectra obtained from MD simulations with predictions from eq 3.

A. Stochastic ENS Equations. In equilibrium, a fluctuating quantity A can be written as $A = A_{\mathrm{av}} + \delta A$, where A_{av} is the average part and δA is the fluctuating part. In equilibrium, the average streaming velocity and spin angular velocity are both zero, so $\mathbf{u} = \delta\mathbf{u}$ and $\boldsymbol{\Omega} = \delta\boldsymbol{\Omega}$. The fluctuations are modeled using the stochastic forcing approach.[46] Here an uncorrelated zero mean stochastic force is added to the constitutive relations; see the SI. For example, for the antisymmetric pressure the constitutive relation with stochastic forcing reads

$$\overset{\mathrm{ad}}{\mathbf{P}} = -\eta_r(\nabla\times\delta\mathbf{u} - 2\delta\boldsymbol{\Omega}) + \delta\overset{\mathrm{ad}}{\mathbf{P}}$$

where $\delta\overset{\mathrm{ad}}{\mathbf{P}}$ is the stochastic fluctuating part of the flux.

To a first-order approximation in the fluctuation we have on the left-hand side of eq 3

$$(\rho_{\mathrm{av}} + \delta\rho)\frac{D\delta\mathbf{u}}{Dt} \approx \rho_{\mathrm{av}}\frac{\partial\delta\mathbf{u}}{\partial t} \qquad (4)$$

and

$$(\rho_{\mathrm{av}} + \delta\rho)(I_{\mathrm{av}} + \delta I)\frac{D\delta\boldsymbol{\Omega}}{Dt} \approx \rho_{\mathrm{av}}I_{\mathrm{av}}\frac{\partial\delta\boldsymbol{\Omega}}{\partial t} \qquad (5)$$

In Fourier space the stochastic ENS equations read to first order in the fluctuations for wave vector $\mathbf{k}$

$$\rho_{\mathrm{av}}\frac{\partial\widetilde{\delta\mathbf{u}}}{\partial t} = -i\mathbf{k}\widetilde{p}_{\mathrm{eq}} - \left(\eta_v + \frac{\eta_0}{3} - \eta_r\right)\mathbf{k}(\mathbf{k}\cdot\widetilde{\delta\mathbf{u}}) - (\eta_0 + \eta_r)k^2\widetilde{\delta\mathbf{u}}$$
$$+ 2i\eta_r\mathbf{k}\times\widetilde{\delta\boldsymbol{\Omega}} + i\mathbf{k}\cdot\widetilde{\delta\mathbf{P}} \qquad (6a)$$

$$\rho_{\mathrm{av}}I_{\mathrm{av}}\frac{\partial\widetilde{\delta\boldsymbol{\Omega}}}{\partial t} = 2\eta_r(i\mathbf{k}\times\widetilde{\delta\mathbf{u}} - 2\widetilde{\delta\boldsymbol{\Omega}}) - \left(\zeta_v + \frac{\zeta_0}{3} - \zeta_r\right)\mathbf{k}(\mathbf{k}\cdot\widetilde{\delta\boldsymbol{\Omega}})$$
$$- (\zeta_0 + \zeta_r)k^2\widetilde{\delta\boldsymbol{\Omega}} + i\mathbf{k}\cdot\widetilde{\delta\mathbf{Q}} + 2\widetilde{\delta\overset{\mathrm{ad}}{\mathbf{P}}} \qquad (6b)$$

due to the properties of the divergence operator. The Fourier transform is defined by eq 2 SI. It is convenient here to introduce the following coefficients

$$\eta_t = \eta_0 + \eta_r, \quad \zeta_t = \zeta_0 + \zeta_r, \quad \text{and} \quad \zeta_l = \zeta_v + \frac{4\zeta_0}{3} \qquad (7)$$

where subscript t indicates transverse and subscript l indicates longitudinal. It has been shown[27,42] that $\zeta_t \approx \zeta_l$, and we write

both coefficients as ζ. We may then define the susceptibility as

$$\chi(k^2) = 4\eta_r + \zeta k^2 \tag{8}$$

where $k^2 = \mathbf{k}^2$. We will also drop the subscript av from here on.

We take $\mathbf{k} = (0, k_y, 0)$ and write out the x component of the velocity and the z component of the angular velocity

$$\rho\frac{\partial\widetilde{\delta u}_x}{\partial t} = -\eta_t k^2\widetilde{\delta u}_x + 2i\eta_r k_y\widetilde{\delta\Omega}_z + ik_y\widetilde{\delta P}_{yx} \tag{9a}$$

$$\rho I\frac{\partial\widetilde{\delta\Omega}_z}{\partial t} = -\chi(k^2)\widetilde{\delta\Omega}_z - 2i\eta_r k_y\widetilde{\delta u}_x + ik_y\widetilde{\delta Q}_{yz} + 2\widetilde{\delta P}^{\text{ad}}_z \tag{9b}$$

These two components are both transverse components to the wave vector and are coupled. We also investigate the longitudinal angular velocity component $\widetilde{\delta\Omega}_y$ which is given through

$$\rho I\frac{\partial\widetilde{\delta\Omega}_y}{\partial t} = -\chi(k^2)\widetilde{\delta\Omega}_y + ik_y\widetilde{\delta Q}_{yy} + 2\widetilde{\delta P}^{\text{ad}}_y \tag{10}$$

Note that this longitudinal component is unaffected by the coupling between the linear and spin angular momenta.

We define the following three correlation functions

$$C^{\perp}_{uu}(\mathbf{k}, t) = \frac{\langle\widetilde{\delta u}_x(\mathbf{k}, t)\,\widetilde{\delta u}_x(-\mathbf{k}, 0)\rangle}{V} \tag{11a}$$

$$C^{\perp}_{\Omega u}(\mathbf{k}, t) = \frac{\langle\widetilde{\delta\Omega}_z(\mathbf{k}, t)\,\widetilde{\delta u}_x(-\mathbf{k}, 0)\rangle}{V} \tag{11b}$$

$$C^{\parallel}_{\Omega\Omega}(\mathbf{k}, t) = \frac{\langle\widetilde{\delta\Omega}_y(-\mathbf{k}, t)\,\widetilde{\delta\Omega}_y(-\mathbf{k}, 0)\rangle}{V} \tag{11c}$$

which we denote the transverse velocity autocorrelation function (TVACF), the transverse cross-correlation function (TCCF), and the longitudinal angular velocity autocorrelation function (LAVACF), respectively. By assumption, the fluctuating fluxes are uncorrelated with the velocity and angular velocity, e.g., $\langle\widetilde{\delta P}_{yx}\widetilde{\delta u}_x\rangle = 0$. Thus, by multiplying eqs 9a and 9b by $\delta u_x(-\mathbf{k}, 0)$ and ensemble averaging, we arrive at the differential equation system for the TVACF and the TCCF

$$\rho\frac{\partial C^{\perp}_{uu}}{\partial t} = -\eta_t k^2 C^{\perp}_{uu} + 2i\eta_r k_y C^{\perp}_{\Omega u} \tag{12a}$$

$$\rho I\frac{\partial C^{\perp}_{\Omega u}}{\partial t} = -\chi(k^2)C^{\perp}_{\Omega u} - 2i\eta_r k_y C^{\perp}_{uu} \tag{12b}$$

Similarly, by multiplying eq 10 by $\widetilde{\delta\Omega}_y(-\mathbf{k}, \mathbf{0})$ one has for the LAVACF

$$\rho I\frac{\partial C^{\parallel}_{\Omega\Omega}}{\partial t} = -\chi(k^2)C_{\Omega\Omega} \tag{13}$$

upon ensemble averaging. Now, eqs 12 and 13 can be solved, yielding to second order in the wave vector

$$C^{\perp}_{uu}(\mathbf{k}, t) = \frac{k_B T}{4\rho}(Ik^2(-e^{-\omega_1 t} + e^{-\omega_2 t}) + 4e^{-\omega_2 t}) \tag{14a}$$

$$C^{\perp}_{\Omega u}(\mathbf{k}, t) = -\frac{i2\eta_r k(e^{-\omega_1 t} - e^{-\omega_2 t})}{4\eta_r + (I(\eta_r - \eta_0) + \zeta)k^2} \tag{14b}$$

$$C^{\parallel}_{\Omega\Omega}(\mathbf{k}, t) = \frac{9k_B T}{4\rho I}e^{-\omega_0 t} \tag{14c}$$

where the characteristic frequencies are

$$\omega_0 = \frac{\chi(k^2)}{\rho I},\ \omega_1 = \frac{\chi(k^2) + I\eta_r k^2}{\rho I},\ \text{and}\ \omega_2 = \frac{\eta_0 k^2}{\rho} \tag{15}$$

The prefactors in eqs 14c and 14a are calculated from the first-order approximation in the fluctuations

$$\widetilde{\delta\mathbf{u}}(\mathbf{k}, t) \approx \frac{m}{\rho}\sum_i \mathbf{c}_i e^{-\mathbf{k}\cdot\mathbf{r}_i} \tag{16}$$

where m is the molecular mass, $\mathbf{c}$ the thermal center-of-mass velocity, and $\mathbf{r}_i$ is the center-of-mass position of molecule i. This comes from the definition of the linear momentum density (SI eq 14). Likewise, to a first-order approximation in density fluctuations and moment of inertia $\rho\mathbf{S} \approx \rho I\mathbf{\Omega}$, and from SI eq 29

$$\widetilde{\delta\mathbf{\Omega}}(\mathbf{k}, t) \approx \frac{3m}{2\rho}\sum_i \mathbf{\Omega}_i e^{-\mathbf{k}\cdot\mathbf{r}_i} \tag{17}$$

as $I = 2I_p/3$ where I_p is the principle moment of inertia.[47] By applying the equipartition theorem, one arrives at the prefactors. Equations 16 and 17 also provide a first-order method to calculate the correlation functions in the MD simulations; this method is used here.

It is informative to work in the frequency domain, i.e., to predict the peak frequencies in the corresponding spectra. Applying the Fourier−Laplace transform defined by

$$\mathcal{L}[f](\mathbf{k}, \omega) = \int_0^{\infty} f(\mathbf{k}, t)e^{-i\omega t}\,dt \tag{18}$$

we get

$$C^{\perp}_{uu}(\mathbf{k}, \omega) = -\frac{k_B T}{4\rho}\left(\frac{Ik^2}{\omega_1 + i\omega} - \frac{4 + Ik^2}{\omega_2 + i\omega}\right) \tag{19a}$$

$$C^{\perp}_{\Omega u}(\mathbf{k}, \omega) = -\frac{i2\eta_r k}{\chi(k^2) + I(\eta_r - \eta_0)k^2}\left(\frac{1}{\omega_1 + i\omega} - \frac{1}{\omega_2 + i\omega}\right) \tag{19b}$$

$$C^{\parallel}_{\Omega\Omega}(\mathbf{k}, \omega) = \frac{9k_B T}{4\rho I}\frac{1}{\omega_0 + i\omega} \tag{19c}$$

From eq 19b we can make a very important conclusion, namely,

$$C^{\perp}_{\Omega u}(\mathbf{k}, \omega) \to 0\ \text{for}\ \mathbf{k} \to \mathbf{0} \tag{20}$$

This means that the coupling can be ignored on long length scales. This is also expected as the classical Navier−Stokes theory holds for macroscopic systems where no coupling effect is observed. The relaxation of spin is still governed by the rotational viscosity, but this relaxation does not affect the relaxation of linear momentum controlled by the usual viscous dissipation processes. If we define ω_c as

$$\omega_c = \lim_{\mathbf{k}\to\mathbf{0}}\omega_0 = \frac{4\eta_r}{\rho I} \tag{21}$$

then LAVACF and TVACF are, in the limit of zero wave vector,

$$C_{\Omega\Omega}^{\parallel}(\omega) = \frac{9k_{\mathrm{B}}T}{4\rho I} \frac{1}{\omega_c + i\omega} \quad \text{and}$$

$$C_{uu}^{\perp}(\mathbf{k}, \omega) = \frac{k_{\mathrm{B}}T}{\rho} \frac{1}{\omega_2 + i\omega} (\mathbf{k} \rightarrow \mathbf{0}) \tag{22}$$

Furthermore, for the fluids studied here the effect of the coupling on the TVACF is not large, that is,

$$\left| \frac{Ik^2}{\omega_1 + i\omega} \right| < \left| \frac{4 + Ik^2}{\omega_2 + i\omega} \right| \tag{23}$$

even for wave vectors in the submolecular diameter range, and the limit in eq 22 need not be taken as a strict limit. It is worth noticing that the rotational viscosity η_r is a linear function of the moment of inertia I for sufficiently large I,[43,48] so ω_c is independent of I here.

B. Comparison with Molecular Dynamics. We first compare the predictions from the continuum ENS theory with MD simulation data for the simple diatomic molecule (the dumbbell model) in the supercritical fluid regime. Transport coefficients η_0, ζ, and η_r are listed in Table 1 in the SI.

Figure 2 shows MD data (symbols connected with lines) for imaginary parts of the spectra of the TVACF and LAVACF; normalization is carried out for clarity. The prediction from the continuum theory is plotted as solid blue lines. It is observed that for small wave vectors $k = 2\pi/L$ the continuum prediction is in excellent agreement with the MD data, but it fails for larger wave vectors $k = 20\pi/L$. We emphasize that no fitting is performed, and all relevant parameters are taken from SI Table 1 found from independent simulations and methods. Using typical values for MD units σ, ϵ, and m, the results show that the continuum theory predicts the mechanical spectrum for wavelengths on the order of 2−3 nm and above and time scales on the order of 1−10 ps and above.

For the TVACF, Figure 2(b), the result can be understood from the fluid stress relaxation at zero wave vector as suggested by Bocquet and Charlaix.[2] From the last equation in eq 15, we can define a wave-vector-dependent relaxation time $\tau_2 = 2\pi\rho/(\eta_0 k^2)$. This relaxation time must be larger than the characteristic relaxation time τ_s at zero wave vector for the predictions to hold for $\tau_s < \tau_2$, i.e., for the viscosity to be wave-vector-independent. This means that

$$\frac{\eta_0 \tau_s k^2}{2\pi\rho} < 1 \quad \text{or} \quad k < \sqrt{\frac{2\pi\rho}{\eta_0 \tau_s}} \tag{24}$$

We refer to this as the Bocquet−Charlaix criterion. Estimates for the relaxation time τ_s are given through the shear pressure (or equivalently stress) autocorrelator

$$G(t) = \frac{V}{k_{\mathrm{B}}T} \langle \overset{os}{P_{xy}}(t) \overset{os}{P_{xy}}(0) \rangle \tag{25}$$

where $\overset{os}{P_{xy}}$ is the (x, y) component of the trace tess symmetric part of the pressure tensor. For the dumbbell model $G(t)$ is fully decayed at $\tau_s \approx 3\sigma/(m/\epsilon)^{1/2}$, which gives $k < 1.2\sigma^{-1}$. This is in perfect agreement with the results depicted in Figure 2(b). Alternatively, the relaxation time can be given through the Maxwell relaxation time $\tau_M = \eta_0/G_\infty$ or the viscous relaxation time[49] $\tau_v = \Psi_{1,0}/2\eta_0$, where G_∞ is the infinite shear modulus and $\Psi_{1,0}$ is the first normal stress coefficient. For the diatomic model studied here, $\tau_M \approx \tau_v = 0.05\sigma(m/\epsilon)^{1/2}$ giving $k < 9.4\sigma^{-1}$, which is not what is observed. Therefore, the characteristic decay time that should be used for the Bocquet−Charlaix criterion is the time for the autocorrelation function $G(t)$ to decay fully.
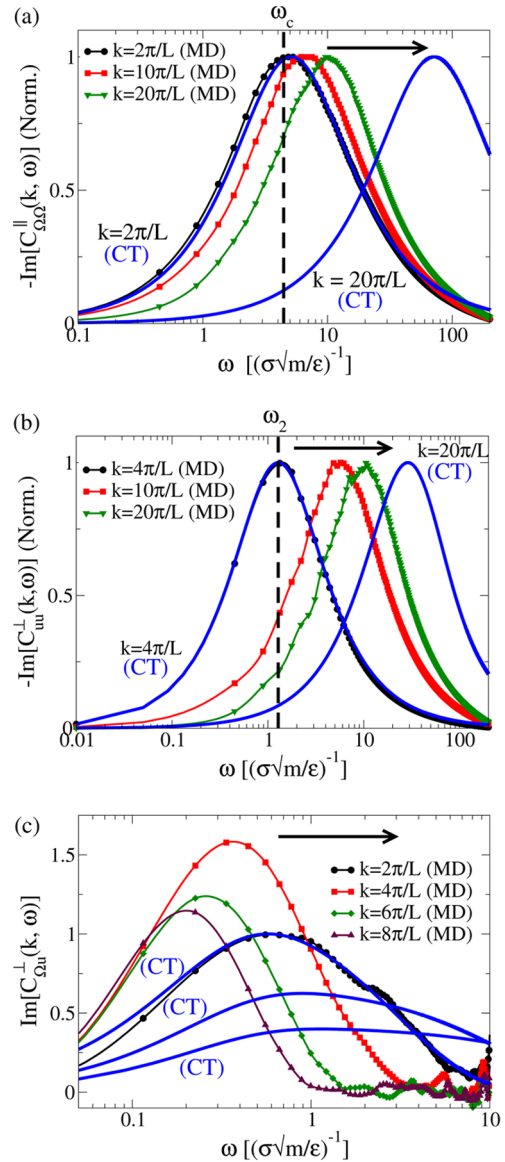
Figure 2. Spectra for the dumbbell model. Blue lines are predictions from the continuum theory (CT) using the coefficients given in Table 1 in the SI all determind by independent simulations. The arrows indicate peak frequency behavior with increasing wave vector. (a) The imaginary part of the spectrum for the longitudinal angular velocity autocorrelation function (LAVACF). Normalization is carried out for clarity in the comparison. The dashed line indicates ω_c given by eq 21. (b) The same as in (a) but for the transverse velocity autocorrelation function (TVACF). The dashed line indicates ω_2 given by eq 15 (c). The same as in (a) but for the transverse cross correlation function (TCCF). The predictions from the theory, eq 14b, for small wave vectors $k \leq 2\pi/L$ are shown. Typical orders of magnitude for the MD units are $\sigma = 1$ Å, $m = 10^{-26}$ kg, and $\epsilon/k_B = 10^2$ K. $L = 13.17\sigma$.

In the small wave vector regime the relaxation of spin angular momentum is dominated by the coupling mechanism between linear and angular momenta as the peak is located at $\omega_0 \approx \omega_c = 4\eta_r/(\rho I)$. The relaxation of linear momentum, Figure 2(b), is on the other hand due to usual viscous mechanisms seen by the peak frequency $\omega_2 = \eta_0 k^2/\rho$. For large k the continuum theory overestimates, by an order of magnitude, the peak frequency for the LAVACF and TVACF due to overestimation of the effect of the spin diffusion.
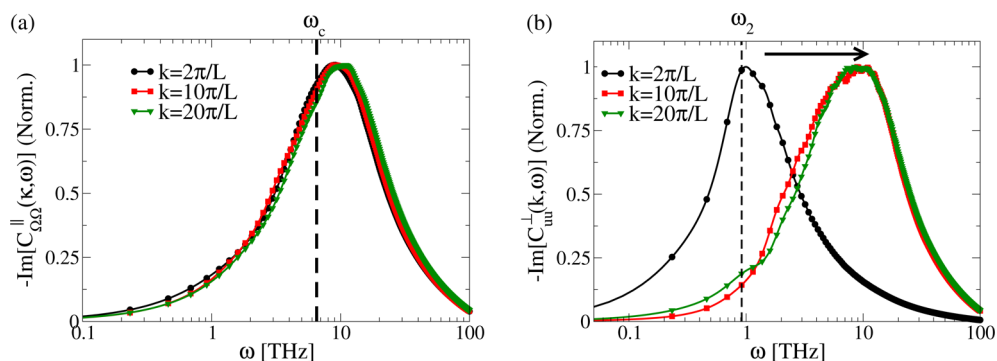
Figure 3. Liquid butane. Molecular dynamics results for (a) the LAVACF spectrum and for (b) the TVACF spectrum. The dashed lines indicate ω_c, eq 21, and ω_2, eq 15. The arrow indicates peak frequency behavior with increasing wave vector. $L = 32.95$ Å.

Figure 2(c) depicts the TCCF for the dumbbell model. Again, the theory performs very well for small wave vectors ($k \leq 2\pi/L$) but fails for larger ones. It is worth noticing that the amplitude of the TCCF is a nonmonotonic function with respect to the wave vector, having a maximum at around $k = 4\pi/L$. This behavior is also captured by the ENS theory. To illustrate that the amplitude is a decreasing function of wave vector, the TCCF for $k = \pi/L$ and $k = \pi/(2L)$ is plotted as predicted by the theory. Recall in the limit $\mathbf{k} \rightarrow 0$ that the coupling vanishes.

Next we apply the theory to liquid butane. As discussed in SI the butane model is not uniaxial or rigid; however, from the principal moment of inertia we argue in SI that the theory should be a good approximation. The result is shown in Figure 3. For the LAVACF one observes a peak frequency at around 9 THz, and the relaxation process is extremely fast. This fast mode is not precisely captured by the theory with $\omega_c = 6.6$ THz. Interestingly, the peak frequency is almost independent of the wave vector for the range studied here. This indicates that for these fast modes the diffusion of spin is less important for the relaxation processes. For the slower relaxation of linear momentum, we see that the peak frequency is predicted well by the theory, the MD result is $\omega = 1.0$ THz, and the predicted one is around $\omega_2 = 0.92$ THz for the lowest wave vector. Again, for larger wave vectors the prediction fails as expected.

III. NONLOCAL RESPONSE

The classical linear constitutive relations are local in the sense that the flux depends only on the local and instantaneous thermodynamic force. This is in general not the case; rather the response depends on the entire force distribution in the system as well as its history. One can model this phenomenologically by introducing frequency- and wave-vector-dependent transport coefficients.[30] The generalized transport coefficients are referred to as kernels. In the homogeneous isotropic case, assuming space and time invariance, the linear nonlocal constitutive relation for the symmetric part of the pressure tensor reads[30,50]

$$\overset{os}{\mathbf{P}}(\mathbf{r}, t) = -\int_{-\infty}^{t} \int_{-\infty}^{\infty} \eta(\mathbf{r} - \mathbf{r}', t - t')\, \overset{os}{\dot{\boldsymbol{\gamma}}}(\mathbf{r}', t)\, d\mathbf{r}'\, dt' \quad (26)$$

$\overset{os}{\dot{\boldsymbol{\gamma}}}(\mathbf{r}, t) = \overset{os}{\nabla}\mathbf{u}(\mathbf{r}, t)$ is the trace-less symmetric part of the velocity gradient, i.e., the strain rate. Fourier transforming with respect to space and Fourier–Laplace transforming with respect to time yields

$$\overset{\widetilde{os}}{\mathbf{P}}(\mathbf{k}, \omega) = -\tilde{\eta}(\mathbf{k}, \omega)\, \overset{\widetilde{os}}{\tilde{\boldsymbol{\gamma}}}(\mathbf{k}, \omega) \quad (27)$$

from the convolution theorem.

The shear viscosity kernel $\tilde{\eta}(\mathbf{k}, \omega)$ can be found from the TVACF as it is now shown. Here we focus on molecules with small moments of inertia and small wave vector regimes, i.e., small Ik^2. In this limit eq 19a can be rearranged to give

$$\tilde{\eta}(\mathbf{k}, \omega) = \frac{k_B T - i\omega\rho C_{uu}^{\perp}(\mathbf{k}, \omega)}{k^2 C_{uu}^{\perp}(\mathbf{k}, \omega)} \quad (\text{small } Ik^2) \quad (28)$$

In particular, we have at zero frequency

$$\tilde{\eta}(\mathbf{k}, 0) = \frac{k_B T}{k^2 C_{uu}^{\perp}(\mathbf{k}, 0)} \quad (\text{small } Ik^2) \quad (29)$$

This approximation holds even for large values of k^2 as discussed above (eq 23). For molecules that can be regarded as point masses, say methane, the moment of inertia is zero and eq 28 is exact. In Figure 4(a) the viscosity kernel at zero frequency is plotted for the methane, dumbbell, butane, and water systems using eq 29. One immediately notices that for $k \approx 1\sigma^{-1}$ the wave-vector-dependent viscosity approaches the zero wave vector limit. This is in good agreement with the Bocquet–Charlaix criterion (eq 24). Interestingly, this is independent of the specific fluid studied here, and the local constitutive relations can be applied on length scales down to approximately $2\pi/k \approx 2-2.5$ nm.

Is this a general result that applies to all fluidic systems? The answer is no! In Figure 4(b) the zero-frequency viscosity kernel is plotted for the asymmetric dumbbell model for different temperatures. The asymmetry arises due to the mass and Lennard-Jones parameter differences between the two constituent atoms. The asymmetric dumbbell model allows one to probe the dynamics in the highly viscous regime without crystallization occurring.[52] The result shows that for relatively high temperatures the kernel has the same wave vector dependency, but on approaching the viscous regime (lower temperature) the kernel reaches the Newtonian viscosity only at longer length scales. This indicates that the dynamical processes behind the viscous response take place on longer length scales in accordance with the cooperative motion in supercooled liquids.[53] The nonlocal viscous response has also been studied for highly viscous two-component Lennard-Jones systems and polymer melts (refs 31 and 32).

The failure of the local constitutive relation, that is, of Newton's law of viscosity, is very clearly illustrated by Todd et al.[54] for a point-mass Weeks–Chandler–Andersen (WCA) system.[55] In real space the nonlocal description amounts to a convolution of the viscosity kernel and the strain rate distribution (eq 26). In the homogeneous situation where the fluid undergoes a steady shear in the x direction with varying amplitude in the z direction we have one nonzero shear component in the pressure tensor,
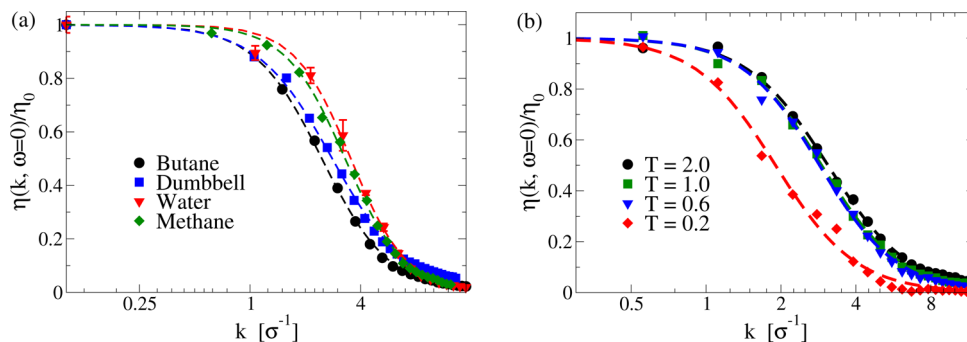
Figure 4. (a) spatial viscosity kernels for the dumbbell model, butane, water, and methane. For butane, water, and methane $\sigma = 3.9233$, 3.166, and 3.80 Å, respectively. (b) Viscosity kernel for the asymmetric dumbbell model at different temperatures. The Newtonian viscosity values are $\eta_0 = 3.2(m\epsilon)^{1/2}/\sigma^2$ for $T = 2.0\epsilon/k_B$ and $\eta_0 = 46(m\epsilon)/\sigma^2$ for $T = 0.2\ \epsilon/k_B$. For (a) and (b) the dashed lines are best fit to the empirical form $\tilde{\eta}(k) = \eta_0/(1 + \alpha k^\beta)$[51] and are included to guide the eye.
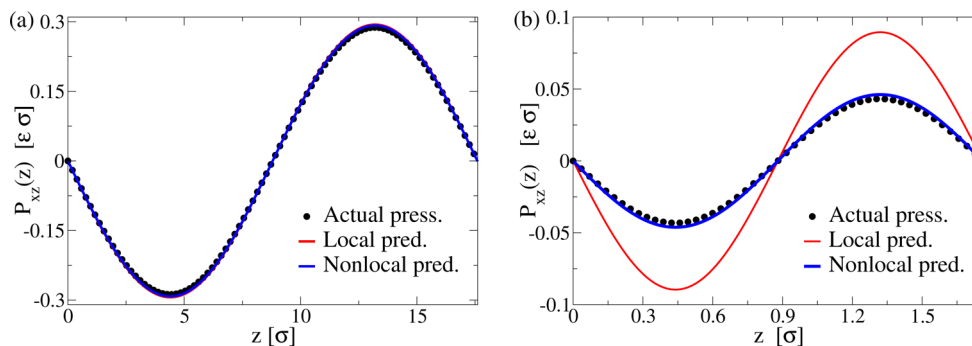
Figure 5. Pressure profiles for the Weeks−Chandler−Andersen point-mass system under periodic shearing force at state point $(\rho, T) = (0.685\sigma^{-3}, 0.765\epsilon/k_B)$. $\alpha = 4.81\sigma^{-2}$ is found from the best fit to data given in ref 56. Input data for the theory is taken from Todd et al.[54] (a) Small wave vector: $k = 0.357\sigma^{-1}$, $\tilde{u}_x^k = 0.887(\epsilon/m)^{1/2}$, $F_0 = 0.15\epsilon/(\sigma m)^{1/2}$. (b) Large wave vector: $k = 3.57\sigma^{-1}$, $\tilde{u}_x^k = 0.027(\epsilon/m)^{1/2}$, $F_0 = 0.225\epsilon/(\sigma m)$.

namely, the P_{xz} component. In this steady situation eq 26 reduces to

$$P_{xz}(z) = -\int_{-\infty}^{\infty} \eta(z - z')\ \dot{\gamma}(z')\ dz' \tag{30}$$

where $\dot{\gamma}(z) = \partial u_x(z)/\partial z$. If the shear is induced by an external force field $F_e(z) = F_0 \cos(kz)$, then the fluid flow is $u_x(z) = \tilde{u}_x^k \cos(kz)$, where $\tilde{u}_x^k$ is the excited Fourier mode amplitude of the velocity field. We assume that this is the only mode excited, i.e., the force amplitude must be sufficiently low.[56] Also, this ensures a linear response as well as constant temperature and density. The strain rate is then

$$\dot{\gamma}(z) = -k\tilde{u}_x^k \sin(kz) \tag{31}$$

For simplicity we shall assume that the kernel is given by a Gaussian function

$$\eta(z) = \eta_0 \sqrt{\frac{\alpha}{\pi}}\ e^{-\alpha z^2} \tag{32}$$

such that $1/\alpha^{1/2}$ gives a characteristic decay length. The kernel must fulfill[54] (i) $\int_{-\infty}^{\infty} \eta(z)\ dz = \eta_0$, and (ii) $\eta(z)$ is an even function. Substituting eqs 31 and 32 into eq 30 we have upon integration

$$P_{xz}(z) = \eta_0 k\tilde{u}_x^k e^{-k^2/4\alpha} \sin(kz) \tag{33}$$

If $\eta(z) = \eta_0\delta(z)$ then the model is local, corresponding to Newton's law of viscosity, that is, for the local model

$$P_{xz}^L(z) = -\eta_0\dot{\gamma} = \eta_0 k\tilde{u}_x^k \sin(kz) \tag{34}$$

The system can be simulated using the sinusoidal transverse force (STF) method,[57] and it is possible to evaluate $\tilde{u}_x^k$ for different external force fields and wave vectors. The two different predictions can be compared to the actual shear pressure P_{xz}^A, which is found directly from the momentum balance equation that for the steady flow reads

$$\frac{\partial}{\partial z}P_{xz}^A(z) = \rho F_e \tag{35}$$

Upon integrating we obtain

$$P_{xz}^A(z) = \frac{\rho F_0}{k} \sin(kz) \tag{36}$$

The comparison is made in Figure 5. Clearly, the local prediction fails for the larger wave vector (Figure 5(b)), whereas the nonlocal prediction agrees with the actual shear pressure. From the nonlocal model we conclude that spatial correlations result in a reduced shear pressure.

From eqs 33 and 34 we can quantitatively evaluate the effect of spatial correlations on the stress. Specifically, we have the relative difference given by

$$\Delta P_{xz}^{rel} = 1 - \frac{P_{xz}}{P_{xz}^L} = 1 - e^{-k^2/4\alpha} \tag{37}$$

For the WCA system studied here $\tau_s \approx 0.6\sigma(m/\epsilon)^{1/2}$, and the Bocquet−Chairlaix criterion gives $k < 2.8\sigma^{-1}$, which corresponds to an error in the local stress up to around 32% according to eq 37.

The Gaussian function does not fit perfectly to the kernel data. Nevertheless, this simple functional form captures the nonlocal response well due to the smoothing of the convolution.

G

Other more complicated functions have been suggested; see refs [31], [51], and [58].

Todd and Hansen[59] showed that the nonlocal response is relevant only for flows where the strain rate is nonlinear with respect to position. Couette and Poiseuille flows are then not affected by nonlocality. To illustrate this consider any functional form for the kernel which fulfills the criteria given above: its integral gives the zero wave vector viscosity, and it is an even function with respect to z. First, making the change in variables $u = z - z'$, eq 30 reads

$$P_{xz}(z) = -\int_{-\infty}^{\infty} \eta(u)\, \dot\gamma(z-u)\, \mathrm{d}u \tag{38}$$

Assuming a strain rate of the form $\dot\gamma(z) = \alpha z$, we have

$$P_{xz}(z) = -\alpha z \int_{-\infty}^{\infty} \eta(u)\, \mathrm{d}u + \alpha \int_{-\infty}^{\infty} \eta(u) u\, \mathrm{d}u = -\alpha\eta_0 z \tag{39}$$

because the integrand in the second integral is an odd function. This result is the same as the local prediction. In general, if a Taylor expansion of the strain rate $\dot\gamma = a_0 + a_1 z + ... + a_n z^n + ...$ exists, then using the properties of odd and even functions one can verify that the nonzero nonlocal effects of the strain rate can be determined by the even moments of the kernel[59]

$$M_n = \int_{-\infty}^{\infty} \eta(z) z^n\, \mathrm{d}z \quad (n > 0 \text{ and even}) \tag{40}$$

In the case of Couette and Poiseuille flows the Taylor expansion terminates at zeroth and first order, respectively, and there are no nonlocal effects.

Finally, the spin and rotational viscosity kernels can be found by simply rearranging eq 19c to give the generalized susceptibility

$$\tilde\chi(\mathbf{k}, \omega) = \frac{\frac{9}{4}k_B T - i\omega\rho I C_{\Omega\Omega}^{\parallel}(\mathbf{k}, \omega)}{C_{\Omega\Omega}^{\parallel}(\mathbf{k}, \omega)} \tag{41}$$

Our group recently[42,43] conjectured that the rotational viscosity η_r governs the fast wave vector independent relaxation processes as indicated in Figures 2(a) and 3(a). This transport coefficient is therefore only frequency-dependent. We then have

$$\tilde\chi(\mathbf{k}, \omega) = 4\tilde\eta_r(\omega) + \tilde\zeta(\mathbf{k}, \omega)k^2 \tag{42}$$

and therefore

$$\tilde\eta_r(\omega) = \frac{1}{4}\lim_{\mathbf{k}\to\mathbf{0}} \tilde\chi(\mathbf{k}, \omega) \quad \text{and} \quad \tilde\zeta(\mathbf{k}, \omega) = \frac{\tilde\chi(\mathbf{k}, \omega) - 4\tilde\eta_r(\omega)}{k^2} \tag{43}$$

We called this the generalized extended Navier−Stokes (GENS) theory. From MD simulations one can calculate the LAVACF (as shown above) and from there find the kernels. For dense fluids $\tilde\zeta$ is characterized by a sharp peak around zero wave vector[42] since the diffusive contribution to the relaxation of the LAVACF is very small for $k > 2\pi/L$; see Figures 2(a) and 3(a). The spin viscosity kernel has the same properties as the shear viscosity kernel, and for this reason we do not expect any nonlocal effects for flows where the gradient of the angular velocity is constant or linear.

IV. NANOFLOWS

Until now we have only considered isotropic and unconfined systems. We will use the information gathered in the next study where the fluids flow in extreme confinements.

A. Poiseuille Flow. We first study a Poiseuille flow; the geometry is shown in Figure 1. In experiments this flow can be achieved by the application of a constant pressure gradient. Generating a pressure difference in simulations with, for example, a piston and using molecular reservoirs can cause density variations in the direction of the flow and other inlet/outlet effects. We therefore use a constant force field acting on each point mass in the fluid to drive the flow. The wall particles are arranged on a simple cubic lattice and are allowed to vibrate around their initial lattice site using a simple restoring spring force. The viscous heating generated in the fluid is removed by thermostatting the wall particles. This method resembles a real physical experiment and is therefore often referred to as direct nonequilibrium molecular dynamics. The interested reader is referred to ref [11] for further details. To get a satisfactory signal-to-noise ratio in the MD simulations, unrealistically large external forces are typically applied to drive the system, and the resulting flow rates are very large, typically on the order of $10-100$ m s^{-1}. Despite these large flow rates the Reynolds number is usually less than unity due to the extremely small characteristic length scales involved. It is very important to ensure that the simulations are carried out in the linear regime, which is discussed below.

1. Continuum Predictions. In the linear regime and for the geometry shown in Figure 1 the ENS equations form a two-point boundary value problem in the steady state

$$\rho F_e + \eta_t \frac{\mathrm{d}^2 u_x}{\mathrm{d}z^2} - 2\eta_r \frac{\mathrm{d}\Omega_y}{\mathrm{d}z} = 0 \tag{44a}$$

$$2\eta_r\left(\frac{\mathrm{d}u_x}{\mathrm{d}z} - 2\Omega_y\right) + \zeta\frac{\mathrm{d}^2\Omega_y}{\mathrm{d}z^2} = 0 \tag{44b}$$

for $-h \leq z \leq h$. Recall that $\eta_t = \eta_0 + \eta_r$ and $\zeta = \zeta_0 + \zeta_r$. Introducing $z' = z/h$, $-1 \leq z' \leq 1$, and applying no-slip boundary conditions, $u_x(-1) = u_x(1) = 0$ and $\Omega_y(-1) = \Omega_y(1) = 0$, Eringen[23] solved this, yielding

$$u_x(z') = u_c\left(1 - z'^2 + \frac{2\eta_r}{\eta_t}\frac{\coth(Kh)}{Kh}\left(\frac{\cosh(Khz')}{\cosh(Kh)} - 1\right)\right) \tag{45a}$$

$$\Omega_y(z') = \frac{u_c}{h}\left(\frac{\sinh(Khz')}{\sinh(Kh)} - z'\right) \tag{45b}$$

with the following definitions of u_c and K

$$u_c = \frac{h^2\rho F_e}{2\eta_0} \quad \text{and} \quad K = \left(\frac{4\eta_r\eta_0}{\zeta\eta_t}\right)^{1/2} \tag{46}$$

The application of the no-slip boundary condition is not justified. A correct treatment applies the Neumann boundary condition for both the velocity and angular velocity fields; however, this is not straightforward in that the two fields are likely coupled. While the boundary condition for the velocity field has been studied in great detail (e.g., refs [60]−[62]), very little is known about the spin boundary condition. Recently De Luca et al.[63] showed that the spin field does possess slippage, and Badur et al.[64] used spin slip to account for flow enhancement. As mentioned in the Introduction, we treat the problem in an ad hoc fashion and set the angular velocity slip in accordance with the MD data.

If one ignores the coupling, $\eta_r = 0$, the solution for the streaming velocity, eq 45a, reduces to the classical Poiseuille flow solution

$$u_x(z') = u_c(1 - z'^2) \tag{47}$$

In this classical situation the angular velocity is found from the vorticity, $\Omega_y = (1/2)\partial u_x/\partial z$, that is,

$$\Omega_y(z') = -\frac{u_c}{h}z' = -\frac{h\rho F_e}{2\eta_o}z' \tag{48}$$

in agreement with eq 45b for $\eta_r \rightarrow 0$. As the classical treatment does not allow for the specification of the spin boundary condition, eqs 45b and 48 differ by order of $h\rho F_e/(2\eta_0)$ at the walls.

From eq 45a one can see that the maximum velocity, located at $z' = 0$, is lowered as a result of the coupling since from the last term we have $1/\cosh(Kh) - 1 < 0$ and thus $u_x(0) < u_c$. A way to quantify this effect is to evaluate the volumetric flow rate Q^3

$$Q = \int_{-w}^{w}\int_{-h}^{h} u_x(z)\,dz\,dy = 2w\int_{-h}^{h} u_x(z)\,dz \tag{49}$$

where w is the half length in the y direction. This gives the relative volumetric flow rate reduction

$$\Delta Q^{\text{rel}} = 1 - \frac{Q}{Q_{\text{class}}} = -\frac{3\eta_r(\tanh(Kh) - Kh)}{\eta_t\tanh(Kh)(Kh)^2} \tag{50}$$

Equation 50 is plotted in Figure 6 for the dumbbell fluid, liquid butane, and water. The relevant coefficients can be found in SI
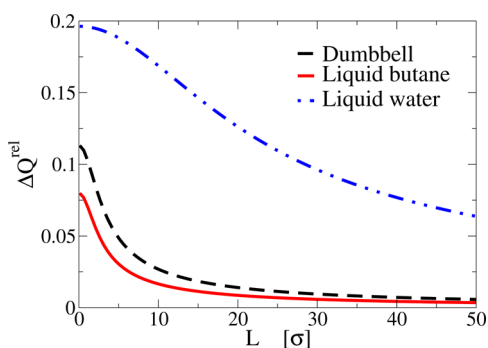
Figure 6. Relative volumetric flow rate for the dumbbell fluid, liquid butane, and liquid water. $\sigma = 3.92$ Å and 3.17 Å for butane and water, respectively.

Table 1. For water flowing in a channel with a width of 9 nm the flow rate is reduced by about 10% due to the coupling. As the channel width increases, the flow rate approaches that of the classical predictions, and the effect of the coupling can be ignored.

From eq 50 the relative flow rate reduction increases as the product Kh decreases. From this observation, one can define a characteristic fluid length scale l_c[65] below which the effect of the coupling becomes significant. To this end we write the parameter K as

$$K = \frac{2}{l_c}\sqrt{\frac{\eta_0}{\eta_t}} \quad \text{with } l_c = \sqrt{\frac{\zeta}{\eta_r}} \tag{51}$$

From SI Table 1 it is seen that $\eta_0 > \eta_r$ and $K \approx 2/l_c$. Thus, a significant flow-rate reduction occurs for fluids with a large critical length scale l_c. For water, $l_c = 3.5$ nm, and for butane, $l_c = 0.5$ nm in agreement with the relative large flow rate reduction observed for water and low reduction for butane.

2. Comparison with Molecular Dynamics Simulations. First we compare MD data with continuum predictions for the dumbbell system. Before the comparison, however, the linear Newtonian response regime should be identified, at least for t

he bulk fluid region. To this end one can apply the SLLOD algorithm developed by Evans and Morris.[66] Basically the method imposes a constant strain rate (linear velocity profile) on the system while ensuring a homogeneous density and isokinetic temperature. To achieve this the equations of motion are reformulated according to the Gaussian principle of least constraint; see also refs 30 and 41. Performing a series of SLLOD simulations it is found that the Newtonian regime occurs in the range of $0 < \dot\gamma < 0.05((m/\epsilon)^{1/2})^{-1}$ for the dumbbell fluid. The upper limit for the external force field can then be approximated by rewriting eq 48 to $\dot\gamma \approx 2\Omega_y = -2u_c/hz'$, giving $F_e < 2\eta_0\dot\gamma_m/\rho h$, with $\dot\gamma_m = 0.05\sigma((m/\epsilon)^{1/2})^{-1}$. Note that in the wall−fluid region the velocity may feature rapid changes, and here the linearity is not guaranteed.

On the basis of the SLLOD approach, Delhommelle[67] developed a method to calculate the rotational viscosity η_r as a function of the spin angular velocity. See also Edberg et al.[68] To our knowledge no synthetic or controlled method exists to study the spin viscosity dependency of the gradient of the spin or the rotational viscosity dependency on the strain rate. We will therefore assume here that the linear regime is identical to the Newtonian regime, i.e., in the regime where the viscosity is independent of the strain rate.

The classical description predicts that the Poiseuille flow is a local flow according to section III. Also, from Figure 6 we expect the flow-rate reduction due to the coupling to be very low for the dumbbell model. Thus, based on the theory we expect the classical description to be a good approximation for this system. The time-averaged velocity and spin angular velocity profiles are shown in Figure 7(a) for the dumbbell model where the pore width is approximately 14.8 atomic diameters. The profiles are sampled after the system reached the steady state. The temperature profile (not shown) is constant, and the temperature is $T = 4.0\epsilon/k_B$ throughout the channel. The predictions from the classical Navier−Stokes theory, eqs 47 and 48, are also plotted using the shear viscosity from SI Table 1. Velocity slippage at the wall−fluid interface is allowed, $u_x(z) = u_c(1 - (z/h)^2) + u_w$; u_w is then the only fitting parameter in the comparison. The agreement between MD data and classical continuum predictions is excellent, except at the wall−fluid interface. This is highlighted by the shear pressures plotted in Figure 7(b). According to the classical theory the shear pressure P_{xz}^{os} is linear; however, at the wall−fluid interface this is not the case. Also, the classical theory assumes a zero antisymmetric part of the shear stress P_y^{ad}. This is clearly not fulfilled near the wall.

To understand the disagreement at the boundary, we analyze the fluid ordering. It is well known that the wall induces a density variation in the fluid.[69] The density profile is shown in Figure 7(c) (black dots). It is seen that the density varies in a region approximately one atomic diameter away from the wall. The transport properties are expected to be functions of density, and one should expect a variation in the viscosities here. Furthermore, one can evaluate the molecular alignment ordering through the parameter[70]

$$p = \frac{3}{2}\cos^2(\theta) - \frac{1}{2} \tag{52}$$

where θ is the angle between the molecular bond and the (x, y) plane. For perfect parallel alignment, $p = -1/2$; that is, the molecules closest to the wall are, on average, aligned with the wall. For distances of around one atomic diameter the molecules are slightly normal to the wall as $p > 0$. The extremes are illustrated
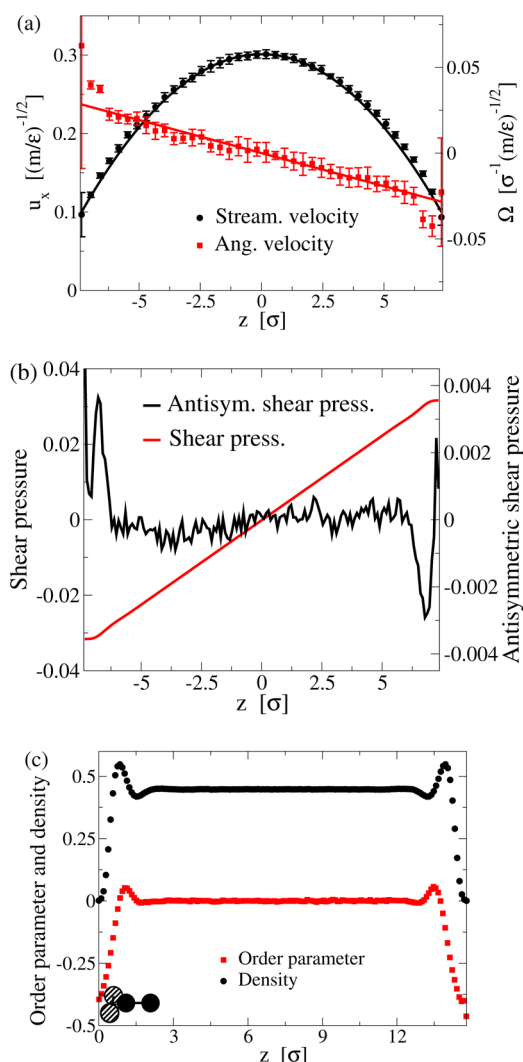
Figure 7. (a) Velocity and angular velocity profiles for the dumbbell model undergoing Poiseuille flow. Symbols represent MD data, and lines represent the classical predictions where slippage is included. (b) Corresponding shear pressures. P_{xz} is calculated by the integration of the momentum balance equation using the density profile given in (c). The antisymmetric pressure is calculated from constitutive relation SI eq 40 using MD data as input. (c) Density and order parameter profiles. The molecules in the lower left corner illustrate (exaggerated) the molecular ordering near the wall.

with the two molecules in the lower left corner in Figure 7(c). For p = 0, the molecules have random orientations, which is the
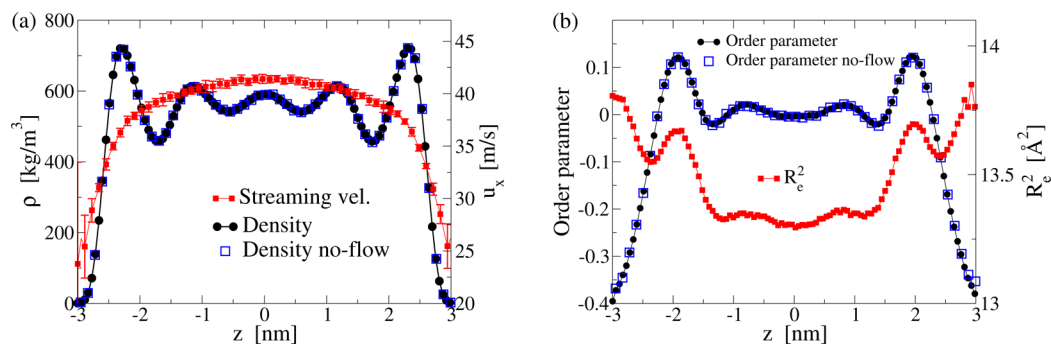
case in the interior of the channel. This means that the system possesses a degree of anisotropy in the wall−fluid region. To fully account for the density variation and ordering one should therefore describe the transport properties through a position-dependent tensorial shear viscosity.

Figure 8(a) shows the velocity and density profiles for a butane flow where the pore width is just 6 nm. For such extreme confinements the fluid layering stretches over the entire pore. The order parameter profile, Figure 8(b), shows that the molecular orientation is strongly anisotropic. Finally, the mean square molecular end-to-end distance R_e^2 also varies, showing that the butane molecule on average is elongated in the fluid-wall region by around 2%. Such a complex system is not modeled appropriately by the classical or extended theories presented here. This is not an indication of a breakdown of the continuum picture but an incomplete modeling. It is worth noting that the fluid ordering and layering are constant over a large range of external forces including zero force (Figure 8) and is thus not flow-induced.

As pointed out by Bitsanis et al.,[71] the velocity profile features surprisingly small modulations considering the density profile: one should expect the transport properties to vary significantly across the channel, having large effects on the flow profile. The authors suggested the local average density model (LADM) wherein the transport properties at a point z are functions of the average density around that point. In the current geometry, where the density is constant in the plane parallel to the wall, the local average density is
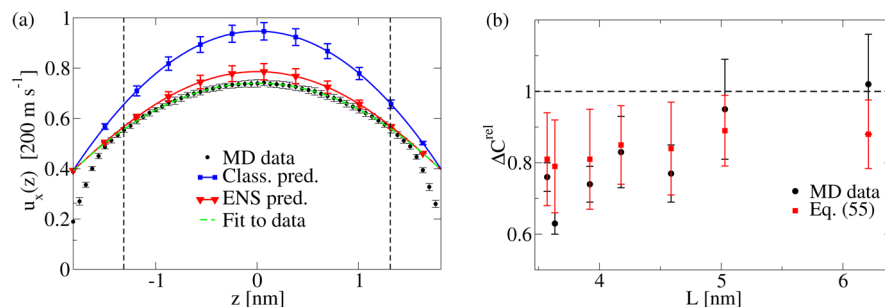
$$\bar{\rho}(z) = \frac{1}{\Delta} \int_{z - \frac{1}{2}\Delta}^{z + \frac{1}{2}\Delta} \rho(z') \, \mathrm{d}z' \tag{53}$$

where Δ defines the region of averaging. The agreement between the LADM and simulation data can be very good, especially if one introduces a nonuniform weighting function.[72] However, the LADM cannot predict the shear pressure response in Figure 5 as the density is constant. Also, the LADM model is not capable of predicting the strain rate reversal observed by Travis et al.[11,73]

To account for the observed velocity profile one can write the position-dependent (inhomogeneous) nonlocal constitutive model as

$$\overset{os}{P}_{xz}(z) = -\int_{-h}^{h} \eta(z, z - z') \, \dot{\gamma}(z') \, \mathrm{d}z' \tag{54}$$

The position dependency reflects the varying density in the wall−fluid region. The application of this relation is not straightforward[74,75] as it is unclear how the convolution should be performed at the wall where the support of the kernel goes

Figure 8. (a) Density and velocity profiles for butane in a slit pore of width 6 nm. The prediction from the theory breaks down and is not shown. (b) Corresponding order parameter and square end-to-end distance profiles.

Figure 9. (a) Velocity profiles of water undergoing Poiseuille flow. (b) Relative profile curvature difference at $z = 0$. From ref 9 with modifications.

beyond the boundary and is unknown.[74,75] Recently, Dalton et al.[76] used a sinusoidal longitudinal force (SLF), also introduced by Hoang and Galliero,[72] to control the density variation in a periodic system. Due to the periodicity, the boundary problem can be eliminated. The density profile can be controlled to such an extent that it resembles that seen in confined systems. The fluid can then be driven by an STF. The authors showed that the nonlocal response is capable of predicting the strain rate reversal observed by Travis et al.[11,73] as well as the relative small modulation in the velocity profile. A rigorous and general implementation of eq 54 into the balance equations for confined systems is still lacking.

For the dumbbell and butane models the coupling between the linear and spin angular velocities has little effect on the flow. From Figure 6, however, the effect is significant for water flow in a channel with widths below 5 nm. In Figure 9(a) MD data for the velocity profile for water is plotted where the channel width is approximately 10 water molecule diameters. Also shown are the predictions from the classical NS and ENS theories. Density and order parameter profiles (not plotted here) show little density variation and molecular alignment, except within 3−4 Å of the wall. The slip velocities are estimated by fitting a second-order polynomial (dashed lines) to the velocity profile, excluding the wall−fluid region where the fluid is slightly anisotropic and inhomogeneous; this then amounts to the apparent slip length[77] and is the only fitting parameter used in the comparison. It is seen that the classical prediction fails, while the ENS theory much better captures the flow profile. Note that the fit of the profile data to the classical description will result in the wrong viscosity no matter how many data points in the wall−fluid region are included. No shift in the profile will change this. An extra source of dissipation must be present. Furthermore, note that a complete description involves a position-dependent nonlocal anisotropic modeling of the wall−fluid region.

To remove any effect in the boundary region one can evaluate the curvature in the channel midpoint, $z = 0$. The predictions are simply found from the second-order derivatives of eqs 45a and 47. The relative difference is

$$\Delta C^{\text{rel}} = 1 - \frac{\eta_r \coth(Kh)Kh}{(\eta_r + \eta_0)\cosh(Kh)} \tag{55}$$

ΔC^{rel} is plotted in Figure 9(b) together with the results from the MD simulations. Within statistical uncertainty the ENS theory and MD simulation results agree. As the channel width increases, the relative curvature difference vanishes and the classical description is recaptured.

The particular model applied is parametrized with respect to the liquid state, and the wall is a Lennard-Jones cubic lattice;

see ref 9. The fluid structure near the wall and its effect on the dynamics will be affected by the different models, choice of model parameters, and wall details. However, it is not the aim here to critically review the fine fluid structure near the wall but to investigate the effect of the coupling.

B. Inserting Torque. Perhaps the most clear illustration of the translational−rotational coupling is seen by introducing an external torque into the system while having a zero production term for the linear momentum. In general, if the resulting torque density $\rho\Gamma_e$ is sufficiently small, then for the geometry in Figure 1 we have

$$\eta_t \frac{d^2 u_x}{dz^2} - 2\eta_r \frac{d\Omega_y}{dz} = 0 \tag{56a}$$

$$\rho\Gamma_e + 2\eta_r\left(\frac{du_x}{dz} - 2\Omega_y\right) + \zeta\frac{d^2\Omega_y}{dz^2} = 0 \tag{56b}$$

Upon integrating eq 56a we get du_x/dz in terms of Ω_z, which is substituted into eq 56b, resulting in a second-order inhomogeneous differential equation for Ω_z. From this and eq 56a and by application of Dirichlet's no-slip boundary conditions one has

$$u_x(z') = \frac{4\eta_r}{\eta_t K}C_1\sinh(Khz') - \left(\frac{2\eta_r(\rho\Gamma\eta_t + 2\eta_r C_0)h}{\eta_t^2\zeta K^2} - \frac{C_0 h}{\eta_t}\right)z' \tag{57a}$$

$$\Omega_y(z') = 2C_1\cosh(Khz') - \frac{\rho\Gamma\eta_t - 2\eta_r C_0}{\zeta\eta_t K^2} \tag{57b}$$

where C_0 and C_1 are integration constants. One can show that C_1 goes rapidly to zero as h increases. In this limit the spin angular velocity is

$$\Omega_y(z') = -\frac{\rho\Gamma_e}{\zeta K^2} - \frac{4\rho\Gamma_e\eta_r^2\eta_t K}{(\eta_t\zeta K^2)^2 - 4\eta_r\eta_t\zeta K^3} \quad (\text{large } h) \tag{58}$$

and the velocity profile is linear with a slope given by the last term in eq 57a. Figure 10 depicts the two profiles for the butane liquid using $\Gamma_e = 413$ m^2 s^{-2}. From this, one sees that the external torque produces a significant local flow; the average flow is zero due to the system symmetry.

In 2009, Bonthuis et al.[78] showed that the coupling between the linear momentum and spin could be exploited in order to pump water through carbon nanotubes by the application of a rotating field. The theory was based on the ENS equations and it was noted that in order to obtain a nonzero mean flow, asymmetric boundary conditions must be employed which can be achieved by confining the fluid between two walls with different hydrophobicities in the case of water pumping. Recently De Luca et al.[63] performed extensive MD simulations of the
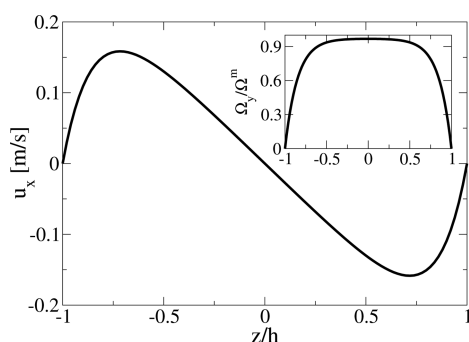
Figure 10. Flow of butane as a result of applying an external torque. The inset shows the corresponding angular velocity normalized with respect to the value in the limit of large h, eq 58, here denoted as Ω_m.

mechanism under experimentally feasible conditions, indicating that the mechanism is functional. This could prove to be a way to overcome the large hydraulic resistance characterizing nanofluidic flows. Felderhof showed in 2011 that the coupling can also be utilized to perform plane-wave pumping[79] and even propel microrobots.[80]

V. SUMMARY

We have derived the relevant dynamical equations for isotropic nanofluidic flows. The formulation is based on the basic definition of a macroscopic field variable from the corresponding microscopic or molecular variable, and it includes the underlying molecular structure. Two intrinsic nanofluidic phenomena were discussed, namely, (i) the coupling between the spin angular momentum and (ii) the linear momentum and the nonlocal fluid response. The important points are the following.

(1) The effect of the coupling between the linear and spin angular velocities can be estimated through the characteristic length scale, l_c, eq 51. For large l_c a significant flow rate reduction is observed, partly explaining the "increased" or "effective" viscosity reported in the literature.[13,14] For polar molecular systems such as water, $l_c \approx 3-4$ nm, and the coupling must be considered on these length scales. For the nonpolar fluids studied here l_c is below 1 nm, and the coupling effect is very small in most situations.

(2) In general any fluid response can be described phenomenologically through a transport kernel that incorporates the spatial and temporal correlation effects. A method for calculating the shear viscosity kernel was presented. This showed that for nonhighly viscous fluids the Newtonian limit is reached on length scales of a few nanometers. This is in agreement with the Bocquet–Charlaix criterion if the complete decay time for the stress autocorrelation function is applied as the relaxation parameter. Importantly, nonlocal effects are not present in simple flows where the strain rate is linear with respect to the spatial coordinate, which is the case for Couette and Poiseuille flows. For nonlinear flows the nonlocal response significantly affects the fluid stress for strain-rate variations on the atomic length scale.

(3) For highly confined fluids, molecular alignment phenomena and molecular deformation can occur along with fluid layering; see Figure 8. Simple classical continuum theory does not include or account for such complex fluid structure. It would be interesting to investigate this in more detail, for example, using the theory for liquid crystals.[70,81]

We conclude that continuum theory is applicable even on the nanoscale if the relevant physical processes are modeled appropriately.

■ ASSOCIATED CONTENT

Ⓢ Supporting Information

The Supporting Information is available free of charge on the ACS Publications website at DOI: 10.1021/acs.langmuir.5b02237.

Balance equations and the extended Navier–Stokes equation. Schematic illustration of the interactions between two molecules i and j. (PDF)

■ AUTHOR INFORMATION

Corresponding Author
*E-mail: jschmidt@ruc.dk.

Notes
The authors declare no competing financial interest.

Biographies

Jesper S. Hansen holds a master's degree in mathematics and chemistry and received his Ph.D. in soft condensed matter in 2003. He has held postdoctoral positions at Universitee Pierre et Marie Curie, Swinburne University of Technology, and Roskilde University. His main research focus area is on nanofluidics, structure and dynamics in liquids and fluids, and reaction–diffusion systems. His interest also includes scientific computing, and he is the author of the introductory book "GNU Octave Beginner's Guide". He is currently an associate professor in physics at Roskilde University.
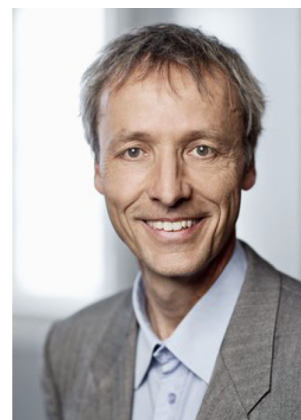
Jeppe C. Dyre is a professor of physics at Roskilde University. After studying mathematics and physics at the University of Copenhagen, he has been with Roskilde University since 1984, from which he in 1987 received his Ph.D. in theoretical physics. Originally interested in solid-state diffusion, ac electrical conduction in disordered solids,

nonlinear response theory, and rheology, he has for many years worked on the physics of highly viscous liquids and the glass transition. Since 2005 he has directed the theoretical and experimental DNRF Centre "Glass and Time", the research of which has gradually expanded from focusing exclusively on glass-forming liquids to including the structure and dynamics of liquids and solids in general. He is a member of the Royal Danish Academy of Sciences and Letters.

Peter Daivis received his undergraduate and masters degrees in applied physics at RMIT University, a graduate diploma in applied colloid science at Swinburne University, and a Ph.D. in physics at Massey University (New Zealand). After completing his Ph.D., he was appointed to a postdoctoral position at the Australian National University. In 1995, he returned to RMIT University, where he has been a professor of physics since 2011. His research has included experimental, computational, and theoretical studies of soft matter, and his current research interests are centred on nonequilibrium statistical and thermal physics, computational nanofluidics, and generalized hydrodynamics.

Billy D. Todd did his undergraduate and postgraduate studies in physics in Australia. He then completed postdoctoral appointments at the University of Cambridge and the Australian National University before moving to CSIRO in Melbourne in 1996. In 1999 he took up an academic appointment at Swinburne University of Technology, where he is currently a professor and Chair of the Department of Mathematics. His research speciality is in statistical mechanics, nonequilibrium molecular dynamics, and computational nanofluidics. He is a fellow of the Australian Institute of Physics and a former president of the Australian Society of Rheology.

Henrik Bruus received his Ph.D. in physics from Niels Bohr Institute, University of Copenhagen, in 1990, and then worked as a postdoctoral researcher at Nordic Institute of Theoretical Physics (1990−1992), Yale University (1992−1994), and CNRS Grenoble (1994−1996). He returned to the Niels Bohr Institute as an associate professor (1997−2001) before moving to the Technical University of Denmark in 2001. There, he became full professor of lab-chip systems in 2005 and of theoretical physics in 2012. His current research interests comprise micro/nanofluidics, acoustofluidics, electrokinetics, the physics of on-chip cell manipulation, the motion of sugar in living plants, and topology-optimized microflows. He has written the monographs "Many-Body Quantum Theory in Condensed Matter Physics" (Oxford University Press, 2004) and "Theoretical Microfluidics" (Oxford University Press, 2008) and is an elected fellow of the American Physical Society.

■ REFERENCES

(1) Eijkel, J. C. T.; van den Berg, A. Nanofluidics: what is it and what can we expect from it? *Microfluid. Nanofluid.* **2005**, *1*, 249−267.

(2) Bocquet, L.; Charlaix, E. Nanofluidics, from bulk to interface. *Chem. Soc. Rev.* **2010**, *39*, 1073.

(3) Bruus, H. *Theoretical Microfluidics*; Oxford University Press, 2008.

(4) Persson, F.; Thamdrup, L. H.; Mikkelsen, M. B. L.; Skafte-Pedersen, P.; Jaarlgard, S. E.; Bruus, H.; Kristensen, A. Double thermal oxidation scheme for the fabrication of SiO_2 nanochannels. *Nanotechnology* **2007**, *18*, 245301.

(5) Landau, L. D., Lifshitz, E. M. *Fluid Mechanics*, 2nd ed.; Elsevier: Amsterdam, 1987.

(6) Tritton, D. J. *Physical Fluid Dynamics*; Oxford Science Publications, 1988.

(7) Lautrup, B. *Physics of Continuous Matter*; Institute of Physics Publishing, Bristol, 2005.

(8) Rowley, R. L.; Painter, M. M. Diffusion and viscosity equation of state for a Lennard-Jones fluid obtained from molecular dynamics simulations. *Int. J. Thermophys.* **1997**, *18*, 1109.

(9) Hansen, J. S.; Dyre, J. C.; Daivis, P. J.; Todd, B. D.; Bruus, H. Nanoflow hydrodynamics. *Phys. Rev. E* **2011**, *84*, 036311.

(10) Thamdrup, L. H.; Persson, F.; Bruus, H.; Flyvbjerg, H. K.; Kristensen, A. Experimental investigation of bubble formation during capillary filling of SiO_2 nanoslits. *Appl. Phys. Lett.* **2007**, *91*, 163505.

(11) Travis, K. P.; Todd, B. D.; Evans, D. J. Depature from Navier-Stokes hydrodynamics in confined liquids. *Phys. Rev. E: Stat. Phys., Plasmas, Fluids, Relat. Interdiscip. Top.* **1997**, *55*, 4288−4295.

(12) Detcheverry, F.; Bocquet, L. Thermal fluctuations in nanofluidic transport. *Phys. Rev. Lett.* **2012**, *109*, 024501.

(13) Gupta, S. A.; Cochran, H. D.; Cummings, P. T. Nanorheology of liquid alkanes. *Fluid Phase Equilib.* **1998**, *150−151*, 125.

(14) Karniadakis, G., Beskok, A., Aluru, N. *Microflows and Nanoflows: Fundamentals and Simulation*; Springer: New York, 2005.

(15) Lukaszewics, G. *Micropolar Fluids: Theory and Applications*; Birkhauser: Boston, 1999.

(16) Eremeyev, V. A., Lebedev, L. P., Altenbach, H. *Foundation of Micropolar Mechanics*; Springer, 2013.

(17) Cosserat, E.; Cosserat, F. Sur la théorie de l'esticité. *Ann. Toulouse* **1896**, *10*, 1.

(18) Cosserat, E., Cosserat, F. *Théorie des Corps d'Eformables*; Hermann, 1909.

(19) Sonnet, A. M.; Maffettone, P. L.; Virga, E. G. Continuum theory for nematic liquid crystals with tensorial order. *J. Non-Newtonian Fluid Mech.* **2004**, *119*, 51.

(20) Muthu, P.; Rathish Kumar, B. V.; Chandra, P. A study of micropolar fluid in an annular tube with application to blood flow. *J. Mech. Med. Biol.* **2008**, *8*, 561.

(21) Grad, H. Statistical mechanics, thermodynamics and fluid dynamics of systems with an arbitrary number of integrals. *Comm. Pure. Appl. Math.* **1952**, *5*, 455.

(22) Dahler, J. S.; Scriven, L. E. Theory of structured continua i. general considerations of angular momentum and polarization. *Proc. R. Soc. London, Ser. A* **1963**, *275*, 504.

(23) Eringen, A. C. *Contribution to Mechanics*; Abir, D., Ed.; Pergamon: Oxford, U.K., 1969 .

(24) de Groot, S. R., Mazur, P. *Non-Equilibrium Thermodynamics*; Dover Publications, 1984.

(25) Snider, R. F.; Lewchuk, K. S. Irreversible thermodynamics of a fluid system with spin. *J. Chem. Phys.* **1967**, *46*, 3163.

(26) Ailawadi, N. K.; Berne, B. J.; Forster, D. Hydrodynamics and Collective Angular-momentum Fluctuations in molecular Fluids. *Phys. Rev. A: At., Mol., Opt. Phys.* **1971**, *3*, 1462−1472.

(27) Evans, D. J.; Streett, W. B. Transport properties of homonuclear diatomics II. Dense fluids. *Mol. Phys.* **1978**, *36*, 161−176.

(28) Alley, W. E.; Alder, B. J. Generalized transport coefficients for hard spheres. *Phys. Rev. A: At., Mol., Opt. Phys.* **1983**, *27*, 3158.

(29) Boon, J. P., Yip, S. *Molecular Hydrodynamics*; Dover Publications: New York, 1991.

(30) Evans, D. J., Morriss, G. P. *Statistical Mechanics of Nonequilibrium Liquids*; Academic Press, 1990.

(31) Furukawa, A.; Tanaka, H. Nonlocal nature of the viscous transport in supercooled liquids: Complex fluid approach to supercooled liquids. *Phys. Rev. Lett.* **2009**, *103*, 135703.

(32) Puscasu, R. M.; Todd, B. D.; Daivis, P. J.; Hansen, J. S. Nonlocal viscosity of polymer melts approaching their glassy state. *J. Chem. Phys.* **2010**, *133*, 144907.

(33) Allen, M. P., Tildesley, D. J. *Computer Simulation of Liquids*; Clarendon Press: New York, 1989.

(34) Wu, Y.; Tepper, H. L.; Voth, G. A. Flexible simple point-charge water model with improved liquid-state properties. *J. Chem. Phys.* **2006**, *124*, 024503.

(35) Ryckaert, J.-P.; Bellemans, A. Molecular Dynamics of Liquid Alkanes. *Faraday Discuss. Chem. Soc.* **1978**, *66*, 95.

(36) Wang, J.; Wolf, R. M.; Caldwell, J. W.; Kollman, P. A.; Case, D. A. Development and Testing of a General Amber Force Field. *J. Comput. Chem.* **2004**, *25*, 1157.

(37) Hansen, J. S. https://code.google.com/p/seplib/.

(38) Thomas, J. A.; McGaughey, J. H. Reassessing Fast Water Transport Through Carbon Nanotubes. *Nano Lett.* **2008**, *8*, 2788−2793.

(39) Whitby, M.; Cagnon, L.; Thanou, M.; Quirke, N. Enhanced fluid flow through nanoscale carbon pipes. *Nano Lett.* **2008**, *8*, 2632.

(40) Irving, J. H.; Kirkwood, J. G. The statistical mechanical theory of transport processes. iv. the equations of hydrodynamics. *J. Chem. Phys.* **1950**, *18*, 817−829.

(41) Todd, B. D.; Daivis, P. J. Homogeneous non-equilibrium molecular dynamics simulations of viscous flow: techniques and applications. *Mol. Simul.* **2007**, *33*, 189.

(42) Hansen, J. S.; Daivis, P. J.; Dyre, J. C.; Todd, B. D.; Bruus, H. Generalized extended Navier-Stokes theory: Correlations in molecular fluids with intrinsic angular momentum. *J. Chem. Phys.* **2013**, *138*, 034503.

(43) Hansen, J. S. Generalized extended navier-stokes theory: Multiscale spin relaxation in molecular fluids. *Phys. Rev. E* **2013**, *88*, 032101.

(44) Kadanoff, L. P.; Martin, P. C. Hydrodynamic Equations and Correlation Functions. *Ann. Phys.* **2000**, *281*, 800.

(45) Onsager, L. Reciprocal relations in irreversible processes. I. *Phys. Rev.* **1931**, *37*, 405.

(46) de Zárate, J. M. O., Sengers, J. V. *Hydrodynamic Fluctuations*; Elsevier: Amsterdam, 2006.

(47) Sarman, S. Flow properties of liquid crystal phases of the gay-berne fluid. *J. Chem. Phys.* **1998**, *108*, 7909.

(48) Moore, R. J. D.; Hansen, J. S.; Todd, B. D. Rotational viscosity of linear molecules: an equilibrium molecular dynamics study. *J. Chem. Phys.* **2008**, *128*, 224507.

(49) Hartkamp, R.; Daivis, P. J.; Todd, B. D. Density dependence of the stress relaxation function of a simple liquid. *Phys. Rev. E* **2013**, *87*, 0321551.

(50) Puscasu, R. M.; Todd, B. D.; Daivis, P. J.; Hansen, J. S. An extended analysis of the viscosity kernel for monatomic and diatomic fluids. *J. Phys.: Condens. Matter* **2010**, *22*, 195105.

(51) Hansen, J. S.; Daivis, P. J.; Travis, K. P.; Todd, B. D. Parameterization of the nonlocal viscosity kernel for an atomic fluid. *Phys. Rev. E* **2007**, *76*, 041121.

(52) Schrøder, T. B.; Pedersen, U. R.; Bailey, N. P.; Toxvaerd, S.; Dyre, J. C. Hidden scale invariance in molecular van der waals liquids: A simulation study. *Phys. Rev. E* **2009**, *80*, 041502.

(53) Cavagna, A. Supercooled liquids for pedestrians. *Phys. Rep.* **2009**, *476*, 51.

(54) Todd, B. D.; Hansen, J. S.; Daivis, P. J. Nonlocal shear stress for homogeneous fluids. *Phys. Rev. Lett.* **2008**, *100*, 195901−195904.

(55) Weeks, J. D.; Chandler, D.; Andersen, H. C. Role of repulsive forces in determining the equilibrium structure of simple liquids. *J. Chem. Phys.* **1971**, *54*, 5237−5247.

(56) Hansen, J. S.; Daivis, P. J.; Todd, B. D. Local linear viscoelasticity of confined fluids. *J. Chem. Phys.* **2007**, *126*, 144706.

(57) Gosling, E. M.; McDonald, I. R.; Singer, K. On the calculation by molecular dynamics of the shear viscosity of a simple fluid. *Mol. Phys.* **1973**, *26*, 1475.

(58) Travis, K. P.; Searles, D. B.; Evans, D. On the wavevector dependent shear viscosity of a simple fluid. *Mol. Phys.* **1999**, *97*, 415.

(59) Todd, B. D.; Hansen, J. S. Nonlocal viscous transport and the effect on fluid stress. *Phys.Rev.E* **2008**, *78*, 051702.

(60) Navier, C. L. M. H. Memoire sur les Lois du Mouvement des Fluids. *Memoires de l'Academic Royale des Sciences de l'Institut de France* **1823**, *6*, 389−440.

(61) Bocquet, L.; Barrat, J.-L. Hydrodynamic boundary conditions, correlations functions, and Kubo relations for confined fluids. *Phys. Rev. E: Stat. Phys., Plasmas, Fluids, Relat. Interdiscip. Top.* **1994**, *49*, 3079−3092.

(62) Hansen, J. S.; Todd, B. D.; Daivis, P. J. Prediction of fluid velocity slip at solid surfaces. *Phys. Rev. E* **2011**, *84*, 016313.

(63) de Luca, S.; Todd, B. D.; Hansen, J. S.; Daivis, P. J. Molecular dynamics study of nanoconfined water flow driven by rotating electric fields under realistic experimental conditions. *Langmuir* **2014**, *30*, 3095.

(64) Badur, J.; Ziolkowski, P.; Ziolkowski, P. On the angular velocity slip in nano-flows. *Microfluid. Nanofluid.* **2015**, *19*, 191.

(65) Hansen, J. S.; Daivis, P. J.; Todd, B. D. Viscous properties of isotropic fluids composed of linear molecules: Departure from the classical Navier-Stokes theory in nano confined geometries. *Phys. Rev. E* **2009**, *80*, 046322.

(66) Evans, D. J.; Morris, G. P. Nonlinear-response theory for steady planar couette flow. *Phys. Rev. A: At., Mol, Opt. Phys.* **1984**, *30*, 1528.

(67) Delhommelle, J. Rotational viscosity of uniaxial molecules. *Mol. Phys.* **2002**, *100*, 3479−3482.

(68) Edberg, R.; Evans, D. J.; Morriss, G. P. On the nonlinear Born effect. *Mol. Phys.* **1987**, *62*, 1357.

(69) Toxvaerd, S. The structure and thermodynamics of a solid-fluid interface. *J. Chem. Phys.* **1981**, *74*, 1998−2005.

(70) Gennes, P. G. D., Prost, J. *The Physics of Liquid Crystals*; Claredon Press, 1993.

(71) Bitsanis, I.; Vanderlick, T. K.; Tirrell, M.; Davis, H. T. Tractable molecular theory of flow in strongly inhomogeneous fluids. *J. Chem. Phys.* **1988**, *89*, 3152.

(72) Hoang, H.; Galliero, G. Shear viscosity of inhomogeneous fluids. *J. Chem. Phys.* **2012**, *136*, 124902.

(73) Travis, K. P.; Gubbins, K. E. Poiseuille flow of lennard-jones fluids in narrow slit pores. *J. Chem. Phys.* **2000**, *112*, 1984.

(74) Zhang, J.; Todd, B. D.; Travis, K. P. Viscosity of confined inhomogeneous nonequilibrium fluids. *J. Chem. Phys.* **2004**, *121*, 10778−10786.

(75) Cadusch, P. J.; Todd, B. D.; Zhang, J.; Daivis, P. J. A non-local hydrodynamic model for the shear viscosity of confined fluids: analysis of homogeneous kernel. *J. Phys. A: Math. Theor.* **2008**, *41*, 035501.

(76) Dalton, B. A.; Daivis, P. J.; Hansen, J. S.; Todd, B. D. Effects of nanoscale density inhomogeneities on shearing fluids. *Phys. Rev. E* **2013**, *88*, 052143.

(77) Lauga, E., Brenner, M., Stone, H. Microfluidics: The No-Slip Boundary Condition. In *Springer Handbook of Experimental Fluid Mechanics*; Tropea, C., Yarin, A. L., Foss, J. F., Eds.; Springer, 2007.

(78) Bonthuis, J. D.; Horinek, D.; Bocquet, L.; Netz, R. R. Electrohydraulic power conversion in planar nanochannels. *Phys. Rev. Lett.* **2009**, *103*, 144503.

(79) Felderhof, B. U. Efficiency of magnetic plane wave pumping of a ferrofluid through a planar duct. *Phys. Fluids* **2011**, *23*, 092003.

(80) Felderhof, B. U. Self-propulsion of a planar electric or magnetic microbot immersed in a polar viscous fluid. *Phys. Rev. E* **2011**, *83*, 056315.

(81) Sarman, S.; Evans, D. J. Statistical mechanics of viscous flow in nematic fluids. *J. Chem. Phys.* **1993**, *99*, 9021−9036.